Archives of Materials Science and Engineering

Volume 122
Issue 2
August 2023
Pages 78-85

International Scientific Journal
published monthly by the
World Academy of Materials
and Manufacturing Engineering

DOI: 10.5604/01.3001.0053.9595

Experimental study of the fracture of CT specimens printed in PLA as a function of the raster width

O. Aourik*, M. Othmani, A. Chouaf**
Laboratory of Mechanics, Engineering and Innovation, Hassan II University, National School of Electricity and Mechanics, Casablanca, Morocco
* Corresponding e-mail address: oumaima.aourik@ensem.ac.ma
** Corresponding e-mail address: a.chouaf@ensem.ac.ma
ORCID identifier: https://orcid.org/0000-0002-7451-5213 (O.A.);
https://orcid.org/0000-0003-1765-6762 (A.C.)

ABSTRACT

Purpose: The FDM (Fused Deposition Modelling) additive manufacturing process is characterised by a large number of process variables that determine the mechanical properties and quality of the manufactured parts. When printing layer by layer, the filaments constituting the layer are welded on the one hand between them in the same layer and on the other hand between the superimposed layers, this welding develops on the contact surfaces (raster width) along the deposited filaments. The quality of this welding determines the resistance to crack propagation between filaments and between layers. This article aims to study the effect of the width of the raster on the resistance to crack propagation in a structure obtained by FDM.

Design/methodology/approach: We have developed an experimental approach from CT specimens to determine the tensile strength of polylactic acid (PLA) polymers, considering the J-Integral method. And given the complexity of the problem, three cases of raster width (l=0.42 mm, l=0.56 mm and l=0.68 mm) have been treated.

Findings: According to the results obtained (J, Δa), the resistance to crack propagation in the parts printed by FDM seems to be better when the width of the filament is small. Indeed, the energy necessary to break the specimen is relatively greater than in the case of a larger width. This finding was confirmed by comparing the values of J for a given advancement of the crack for the three cases studied.

Research limitations/implications: In order to present an exhaustive study, we focused on the effect of raster widths (including 0.42 mm, 0.56 mm to 0.68 mm) on the crack propagation of printed PLA. This study is in progress for other printing parameters. To highlight the cracking mechanisms, microscopic observations will be developed in greater depth at the SEM.

Practical implications: Our analysis can be used as decision support in the design of FDM parts. In effect, we can choose the raster width that would provide the resistance to crack propagation desired for a functional part.

Originality/value: In this article, we analysed the damage mechanism of CT specimens printed by FDM. This subject represents a new direction for many lines of research. For our study, we used the J-Integral theoretical approach to study the fracture behaviour of these parts by determining the resistance curves (J-Δa).

Keywords: FDM, Raster width, PLA, CT specimen, Crack, (J-Δa) curve
Reference to this paper should be given in the following way:
O. Aourik, M. Othmani, A. Chouaf, Experimental study of the fracture of CT specimens printed in PLA as a function of the raster width, Archives of Materials Science and Engineering 122/2 (2023) 78-85. DOI: https://doi.org/10.5604/01.3001.0053.9595

1. Introduction

Additive manufacturing today covers virtually all industrial sectors [1]. Thanks to the maturity of its technique, it is possible to produce parts with very satisfactory appearance performance [2]. However, the performances at the level of mechanical behaviour have been developed but have yet to sufficiently take into account the complexity of the printed structures and their sensitivity to the numerous printing parameters. It has been pointed out that the FDM (Fused Dipositive Modelling) technique, also commonly referred to as FFF (Fused Filament Fabrication), is characterised by a large number of variables to be fixed for the process. These variables determine the mechanical properties and the quality of the manufactured parts [3-5]. The impact of these printing parameters on mechanical properties has been the subject of much research.

Ziemian et al. investigated the effect of construction orientation on the fatigue strength of acrylonitrile butadiene styrene (ABS) parts manufactured by 3D printing [6]. Similar work has been done by Durgun et al. where the effect of raster angle and part orientation on the mechanical properties of ABS printed parts was evaluated using the three-point tensile and bend test [7]. Additionally, Sood et al. also studied the compressive strength of ABS obtained by FDM as a function of construction orientation, raster angle, layer thickness, raster width and spacing [8]. Tymrak et al. have improved the tensile strength and modulus elasticity of printed ABS and PLA parts by changing build orientation, layer thickness and raster gap [5]. In addition to orientation and layer thickness, several other parameters have also been evaluated in previous research. Zhang et al. studied the fracture behaviour of a glass fibre-reinforced polymer seal under tension at different temperatures [9]. Vicente et al. tested in tension the influence of nozzle size on the mechanical properties of parts printed in ABS [4].

Despite this very interesting amount of work on the mechanical performance of printed parts, work on the resistance to crack propagation in this type of structure remains to be further developed.

Indeed, compared to other techniques, the phenomenon of crack propagation in polymer structures obtained by FDM is complex due to their microstructures which strongly depend on various printing parameters [10]. In this sense, we are interested in the damage aspects of parts printed by the FDM technique [11].

We recall that the principle of this process by FDM is based on manufacturing a part layer by layer [12,13]. During this process, the filaments constituting the layer are welded on the one hand between them in the same layer and on the other hand between the superposed layers. This welding develops on the contact surfaces and along the deposited filaments. The quality of this welding determines the resistance to crack propagation between filaments and between layers.

We highlighted this mechanism in our previous study [14]. The result we obtained was confirmed by the work of Ahn et al. [15].

In the present study, we tried to deepen our analysis of this damage by separating contact surfaces between filaments. These surfaces depend mainly on the filament width chosen, which will condition the welding quality between filaments. We considered this width to study its influence on the resistance to crack propagation in a structure obtained by 3D printing (FDM). To do this, we have developed an experimental approach to determine the tensile strength of polylactic acid (PLA) polymers. The type of test adopted is tensile on appropriate CT specimens. In this experimental study, three cases of raster width (l=0.42 mm, l=0.56 mm and l=0.68 mm) were treated.

For each width, we printed three CT specimens. From the tests on these specimens, we determined for each case the curve of resistance by appealing to the concept of the integral J in fracture mechanics.

2. Theoretical approach

To analyse the fracture behaviour of a structure, one must take into account its level of ductility. Indeed, in relation to the ductility of our structure, we must choose one of the two concepts developed to study rupture. The first is Linear Elastic Fracture Mechanics (LEFM) based on the Stress Intensity Factor K and applies only to material with elastic behaviour. On the other hand, for a viscoelastic

material like polymers where the various forms of plastic deformation which appear, before and during the rupture, one considers a second concept based on the elastoplastic mechanics of the rupture (Post Yield Fracture Mechanics – PYFM).

This second concept is based on the formulation of the J-integral, which is the most appropriate for describing ductile failure in a ductile material. Originally, this integral J was expressed from the following relation [16]:

$$J = \oint_{\Gamma} \left(w\, dy - T_i \frac{\partial u_i}{\partial x}\, ds \right) \quad (1)$$

$\oint_{\Gamma}$ is an arbitrary contour surrounding the crack tip, w the strain energy density, T_i stress vector components, u_i displacement vector components, ds the length increment along the contour, and x and y are the Cartesian coordinates with respect to at a chosen landmark.

From this integral J, we will analyse the resistance to cracking in our CT specimens printed in (PLA). To do this, we consider the curve ((J = f(Δa)), which takes into account the effect of the advance of the crack (Δa) as well as nonlinear behaviour. This curve, known as the Resistance curve, describes the energy conditions for crack extension after initiation.

In practice, this energy J can be deduced by experience through the following formula [17]:

$$J = \frac{\eta\, \mathrm{U}}{B\,(W - a_0)} \quad (2)$$

According to ASTM D 6068 [17], the energy required to expand the crack, U, is used to calculate J. The total energy (U_T) is the sum of U and U_i, the indentation energy:

$$J = \frac{\eta (U_T - U_i)}{B\,(\mathrm{W} - a_0)} \quad (3)$$

W is the width of the specimen. η is a geometric dimensionless parameter. Garcia et al [18] claim that to calculate J of polymers, the factor η depends only on the ratio between the length of the crack a_0 and the width of the specimen W (a_0/W).

Clarke and Landes [19] succeeded in obtaining an approximation of η for the CT specimen using the following formula:

$$\eta = 2 + 0.522 \left(1 - \frac{a_0}{w}\right) \quad (4)$$

The approach followed to determine the two energies U_T and U_i is developed in the experimental results section. And from their values, we deduce those of J via equation (3).

3. Experimental approach

The ISO 13586 and ASTM D 5045 standards postulate that the tests must be conducted on CT specimens to evaluate J of a thermoplastic and thermosetting material [20,21]. Although the specifications and recommendations of the two standards ISO 13586 and ASTM D 5045, are only applicable for linear fracture mechanics, the choice and sizing of the specimens have been maintained by the standard ASTM D 6068 for the determination of curves strength of elastoplastic polymer materials. For our experimental study, we, therefore, considered CT specimens with a notch to determine U_T and without a notch to determine U_i [17].

3.1. Realization of specimens by FDM

To produce the CT specimens with a notch (Fig. 1) as well as without a notch, a CAD model was developed according to the FDM manufacturing method. This digital model was converted into a Stereolithography (STL) file and translated into a machine instruction (G-code) file. This file describes the nozzle trajectories that deposit the filling material in the form of the filament. Once the file is obtained, the samples can be made on a 3D printer. The printing parameters adopted are shown in Table 1.

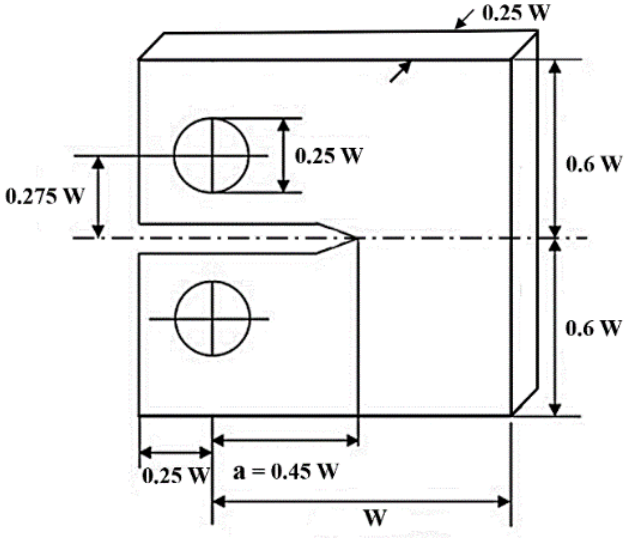

Fig. 1. Dimensions of the CT specimen (W=50.8 mm) ASTM D5045 [21]

We remind you that this FDM printing technique is building successive layers that allow us to control and produce samples with different raster widths. For our study, we considered three cases of width (l=0.42 mm, l=0.56 mm and l=0.68 mm). These widths as well as the contact surfaces between filaments, are shown schematically in Figure 2. On each CT specimen printed on a RAISE 3D type machine, we manually performed the crack initiation using a cutter. A profile projector controlled the depth of this priming.

Table 1.
Considered parameters for its printing

Parameters	Values	Units
Layer thickness	0.2	mm
First-layer printing speed	30	mm/s
Print speed of other layers	150	mm/s
Build orientation	XYZ	
infill pattern	Line	
Raster angle	90	Degree
Infill percentage	100	%
Number of perimeters	2	
Number of bottom/top solid layer	0	
Nozzle Temperature	210	°C
Bed Temperature	60	°C
Filament type	RAISE 3D Cream PLA 1.75 mm	

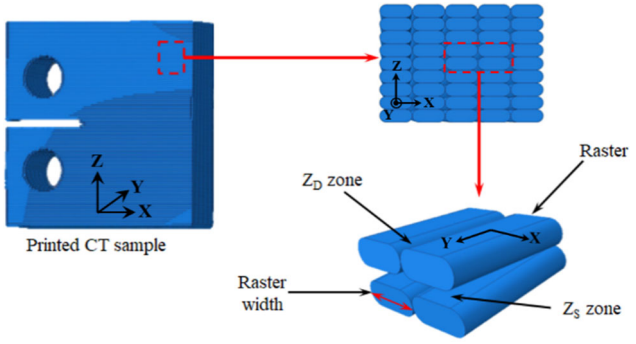

Fig. 2. Raster width of constituting the CT sample, ZD: Contact between adjacent filaments of the same layer, ZS: Contact between filaments of two superimposed layers

3.2. Test procedure

To carry out our experimental tests, we used a traction machine of the MTS810 type (Fig. 3). A well-adapted assembly for our CT specimens was adopted. On each of the specimens, we have set up a graduation in mm to identify the different positions of the tip of the crack. To monitor the crack, we installed a camera connected to a PC designed to record the propagation of the crack.

In compliance with the ISO 13586 standard, we conducted our tests with a speed of 0.5 mm/min and in an ambient environment (T=23°). After each test, three types of data were collected:

- the load-displacement curves which lead to the calculation of the integral J via the relation (3),
- the load-time curves that allow us to follow the crack,
- the follow-up videos of the crack through which we measure its progress Δa as a function of time.

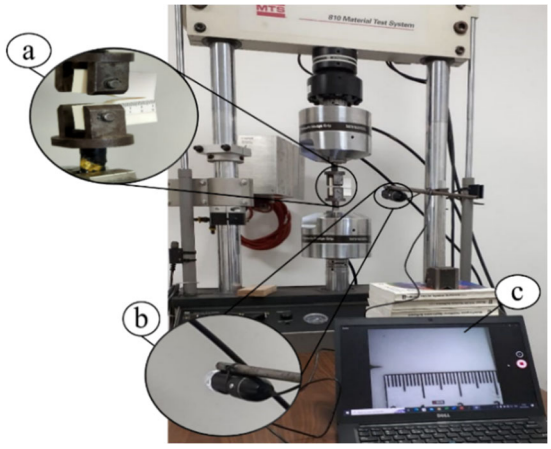

Fig. 3. MTS810 tensile machine: (a) Mounting adapted for CT specimens, (b) Crack propagation monitoring camera and (c) Visual control from graduation in mm of crack propagation

4. Load-displacement curves: CT specimens with and without notch

From our tests, we obtained load-displacement curves for two types of specimens. The first type relates to CT specimens with notch and priming (Fig. 4). The second corresponds to specimens without the notch (Fig. 5). We recall that it is from the results of these two types of specimens that we will deduce, according to the ASTM D 6068 standard, the values of the integral J [17].

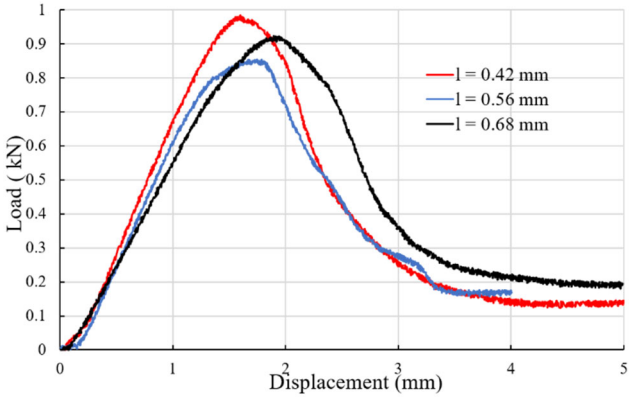

Fig. 4. Load-displacement curves of test specimens with notch for l = 0.42 mm, l = 0.56 mm and 0.68 mm

According to the results of Figure 4, we can see that for the three widths of the filaments studied, the behaviour is relatively similar. This behaviour first passes through a phase of resistance to crack propagation; the load continues

to increase linearly. Then, one can observe a second phase corresponding to the beginning of the propagation of the crack with a very slow evolution. In the last phase, the propagation of the crack is rapid and leads to the final failure. Of the appearance of these curves, it is difficult to clearly distinguish the effect of the width on the resistance to crack propagation.

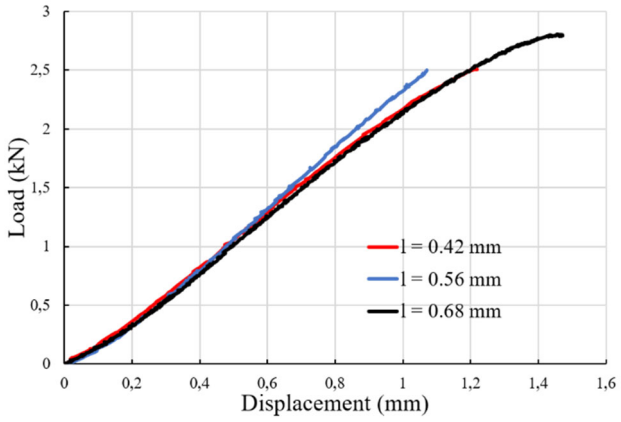

Fig. 5. Load-displacement curves of CT specimens without a notch for l = 0.42 mm, l = 0.56 mm and 0.68 mm

On the other hand, if we are interested in the area under each curve, we can notice small differences between the three cases of widths. As a result, the energies necessary to make the crack propagate are different by comparing the three cases. This observation will be considered to calculate the integral J according to the different energies U_T and U_i, which will be determined from the curves of Figures 4 and 5.

We recall that according to the ASTM D 6068 standard, the curves in Figure 5 which were obtained for test specimens without a notch, allow us to determine the so-called "indentation" energies U_i.

To experimentally determine the energies U_T and U_i, for a given width, we place ourselves on the curves concerned, as shown in Figure 6. From Figure 6a (sample with notch), we determine the energy U_T, which is the area under the curve from zero to the displacement, corresponding to the maximum force F applied to the notched and pre-cracked specimen.

This same force is considered to be determined U_i from Figure 6b (sample without notch). We recall that this quantity of energy is dissipated by phenomena other than cracking. The values of U_T and U_i obtained are grouped in Table 2.

Finally, from the determination of the energies U_T and U_i, J can be calculated for each filament width by equation (3).

5. Resistance curves

For each experimental test, we have recovered the load-time curve as well as the video of the progress of the crack, which the ImageJ software will process to measure Δa at each instant t (Fig. 7).

To plot the resistance curve, which results in the evolution of J as a function of Δa, it is necessary to determine the corresponding energy J for each progression Δa. To do this, we used our video recordings of the propagation of the crack during the tensile test on the CT specimens. With these recordings, we have, for each time t_i, an advancement Δa_i of the crack. And for each t_i corresponds a tensile force F_i which itself corresponds to a displacement d_i. With this force F_i, the energies U_T^i and U_i^i are determined by standing on the curves (F, d) (see Fig. 6). And it is from

Table 2.
Energy values U_T and U_i for each (Δa and F)

			l = 0.42 mm			
Δa, mm	0.148	0.46	0.663	0.784	0.804	--
F, N	530.102	639.630	758.185	850.647	918.397	--
U_T, N*mm	216.647	307.564	428.751	540.385	648.223	--
U_i, N*mm	75.677	105.578	141.028	183.525	204.635	--
			l = 0.56 mm			
Δa, mm	0.794	0.84	0.898	1.033	1.181	1.398
F, N	704.894	767.144	800.081	811.069	826.543	839.234
U_T, N*mm	401.888	489.145	539.333	569.230	619.128	652.698
U_i, N*mm	129.197	145.116	159.194	161.380	180.933	183.712
			l = 0.68 mm			
Δa, mm	0.49	0.685	0.927	1.363	1.521	1.778
F, N	790.739	844.353	863.435	882.435	899.584	921.872
U_T, N*mm	378.832	507.197	625.963	751.006	800.940	896.162
U_i, N*mm	163.231	204.961	233.367	255.534	263.476	273.797

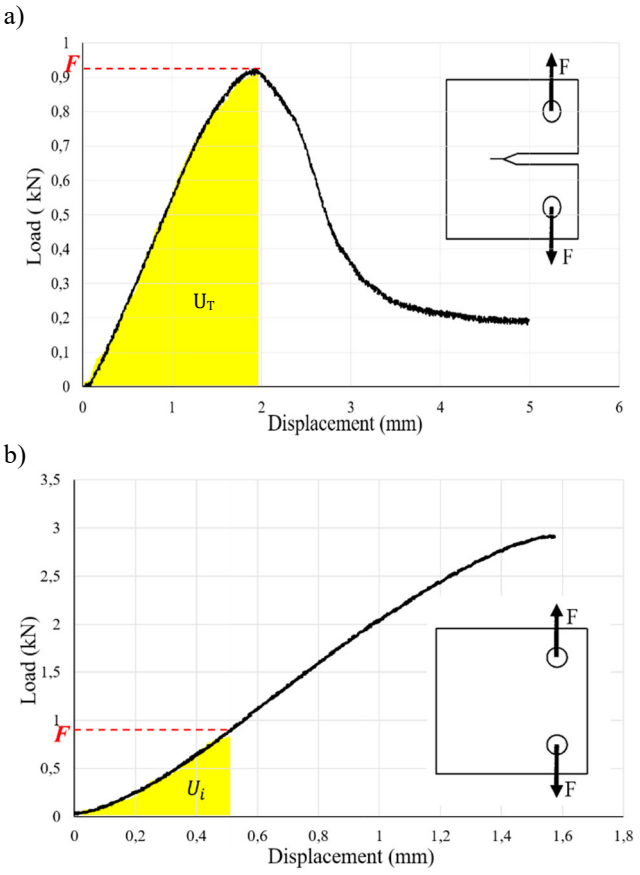

Fig. 6. Areas under the load-displacement curves associated with the energy calculations: a) U_T for CT specimens with a notch and b) U_i for CT specimens without a notch, according to standard ASTM E813 [22]

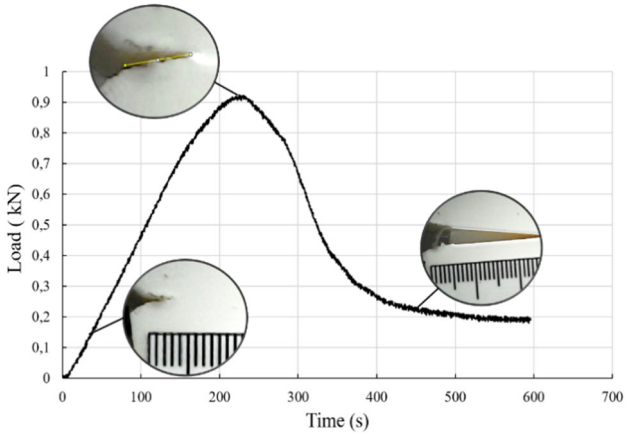

Fig. 7. Determination of the load and the progress of the crack for each instant *t*

these energies U_T^i and U_i^i hat we deduce by formula (3) the value of J_i. Finally, we obtain a series of points (Δa, J_i) from which we can draw the resistance curve as shown in Figure 8.

Through this graph, the points are distributed in a more or less linear form for the three cases of widths studied. To better exploit this graph, we have traced the average rights for each case (Fig. 9).

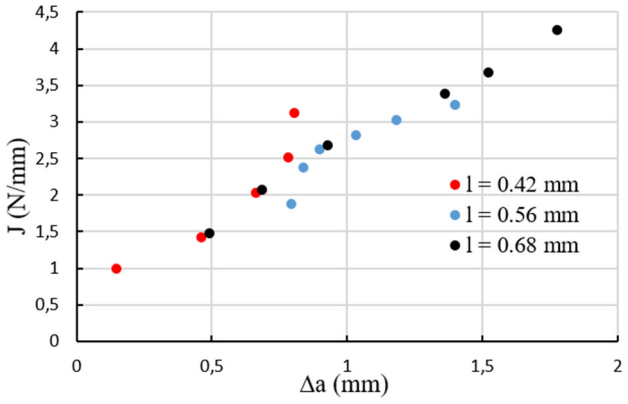

Fig. 8. Variation of energy J as a function of crack advancement Δa for three raster widths (0.42 mm, 0.56 mm and 0.68 mm)

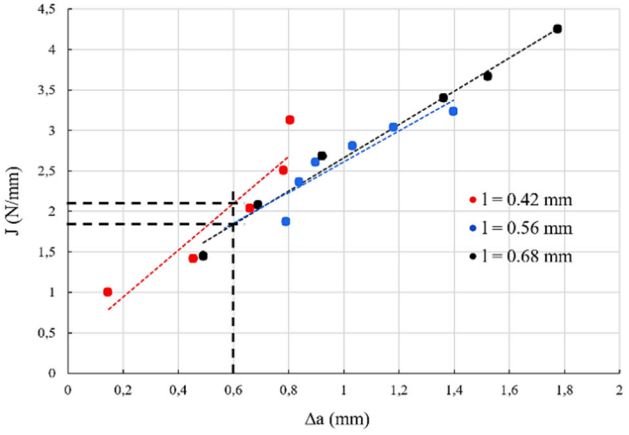

Fig. 9. Mean evolution of energy J as a function of crack advancement Δa for three raster widths (0.42 mm, 0.56 mm, and 0.68 mm)

For the cases of widths l=0.56 mm and l=0.68 mm, the associated straight lines are almost coincident. As a result, the resistance to crack propagation exhibited by these two-width cases is practically similar. On the other hand, for the case l=0.42 mm, the mean line is well-shifted compared to those of the other cases of width. Indeed, the slope of the line for l=0.42 mm is greater compared to those of the widths

l=0.56 mm and l=0.68 mm. With this relatively marked difference, the case of l=0.42 mm seems to generate better resistance to crack propagation.

As an indication, to cause advancement of the crack Δa= 0.6 mm, it is necessary to supply energy of the order of 2.06 N/mm for the case l=0.42 mm. On the other hand, for the cases l=0.56 mm and l=0.68 mm it is necessary to supply only an energy of 1.83 N/mm. Various physical phenomena could explain this difference. Among them, we can mainly cite the phenomenon of cohesion between filaments during manufacturing the part.

The greater the width of the filament, the greater the cohesive contact surface. Therefore, opening and propagating the crack at this contact should require more energy. Indeed, in this case, part of the energy is dissipated at the level of the partial separations between adjacent filaments of the same layer (Fig. 2). This is why damage by the separation of filaments from two superimposed layers requires more energy.

6. Conclusions

In this experimental study, we have highlighted the effect of raster width on the resistance to crack propagation in CT specimens printed in PLA. To do this, we have determined for the cases of widths studied (l=0.42 mm, l=0.56 mm and l=0.68 mm) the resistance curve by appealing to the concept of the integral J in nonlinear fracture mechanics. This energy J was determined from the tensile curves on CT specimens with a notch and without a notch. To determine the progress of the crack Δa for each J, we used a camera to monitor the propagation of the crack as a function of time.

From these resistance curves, we found that the case of the width l=0.42mm presents a better resistance than the other cases (l=0.56 mm and l=0.68 mm).

Indeed, to cause for example an advancing of the crack Δa=0.6 mm, it is necessary to supply an energy of the order of 2.06 N/mm for the case l=0.42 mm. On the other hand, for the cases l=0.56 mm and l=0.68 mm it is necessary to supply only an energy of 1.83 N/mm. For the specimen with l=0.42 mm, part of the energy was dissipated at the level of the partial separations between adjacent filaments of the same layer. This is why damage by separating filaments from two superimposed layers requires more energy.

Based on Table 3, we can assume that our values are comparable to those obtained by Santana et al. (2.38 N/mm) and Majid et al. (2.08 N/mm) [23,24].

Comparing our values more one time to another manufacturing technique as Injection Moulding (IM) [25]. It is generally observed that 3D printed parts exhibit lower toughness compared to IM PLA parts (the fracture toughness was 9.90 N/mm) [26].

Table 3.
Energy values of J for two different building methods

Method	Reference	Average J, N/mm
IM	Gao et al. [26]	9.90
FDM	Aourik et al.	1.83-2.06
FDM	Santana et al. [23]	2.38
FDM	Majid et al. [24]	2.08

This very interesting observation was confirmed by our first observations of the rupture facies, which are the subject of our perspectives of this study. These perspectives will also include the determination of the J_{IC} critical values as well as numerical simulations.

References

[1] R. Winarso, R. Ismail, J. Jamari, A.P. Bayuseno, Application of Fused Deposition Modeling (FDM) on Bone Scaffold Manufacturing Process: A Review, Heliyon 8/11 (2022) e11701. DOI: https://doi.org/10.1016/j.heliyon.2022.e11701

[2] R. Matsuzaki, M. Ueda, M. Namiki, T.K. Jeong, H. Asahara, K. Horiguchi, Y Hirano, Three-dimensional printing of continuous-fiber composites by in-nozzle impregnation, Scientific Reports 6 (2016) 23058. DOI: https://doi.org/10.1038/srep23058

[3] A. Lanzotti, M. Grasso, G. Staiano, M. Martorelli, The impact of process parameters on mechanical properties of parts fabricated in PLA with an open-source 3-D printer, Rapid Prototyping Journal 21/5 (2015) 604-617. DOI: https://doi.org/10.1108/RPJ-09-2014-0135

[4] C.M.S. Vicente, T.S. Martins, M. Leite, A. Ribeiro, L. Reis, Influence of fused deposition modeling parameters on the mechanical properties of ABS parts. Polymers Advanced Technology 31/3 (2020) 501-507. DOI: https://doi.org/10.1002/pat.4787

[5] B.M. Tymrak, M. Kreiger, J.M. Pearce, Mechanical properties of components fabricated with open-source 3-D printers under realistic environmental conditions, Materials and Design 58 (2014) 242-246. DOI: https://doi.org/10.1016/j.matdes.2014.02.038

[6] C. Ziemian, M. Sharma, S. Ziemi, Anisotropic Mechanical Properties of ABS Parts Fabricated by Fused Deposition Modelling, in: M. Gokcek (ed), Mechanical Engineering, IntechOpen, Rijeka, 2012, 159-180. DOI: https://doi.org/10.5772/34233

[7] I. Durgun, R. Ertan, Experimental investigation of FDM process for improvement of mechanical properties and production cost, Rapid Prototyping Journal 20/3 (2014) 228-235. DOI: https://doi.org/10.1108/RPJ-10-2012-0091

[8] A.K. Sood, R.K. Ohdar, S.S. Mahapatra, Experimental investigation and empirical modelling of FDM process

for compressive strength improvement, Journal of Advanced Research 3/1 (2012) 81-90. DOI: https://doi.org/10.1016/j.jare.2011.05.001

[9] Y. Zhang, A.P. Vassilopoulos, T. Keller, Effects of low and high temperatures on tensile behavior of adhesively-bonded GFRP joints, Composite Structures 92/7 (2010) 1631-1639. DOI: https://doi.org/10.1016/j.compstruct.2009.11.028

[10] K.R. Hart, E.D. Wetzel, Fracture behavior of additively manufactured acrylonitrile butadiene styrene (ABS) materials, Engineering Fracture Mechanics 177 (2017) 1-13. DOI: https://doi.org/10.1016/j.engfracmech.2017.03.028

[11] O. Aourik, M. Othmani, B. Saadouki, K. Abouzaid, A. Chouaf, Fracture toughness of ABS additively manufactured by FDM process, Journal of Achievements in Materials and Manufacturing Engineering 109/2 (2021) 49-58. DOI: https://doi.org/10.5604/01.3001.0015.6258

[12] J. Li, S. Yang, D. Li, V. Chalivendra, Numerical and experimental studies of additively manufactured polymers for enhanced fracture properties. Engineering Fracture Mechanics 204 (2018) 557-569. DOI: https://doi.org/10.1016/j.engfracmech.2018.11.001

[13] R. Ghandriz, K. Hart, J. Li, Extended finite element method (XFEM) modeling of fracture in additively manufactured polymers, Additive Manufacturing 31 (2020) 100945. DOI: https://doi.org/10.1016/j.addma.2019.100945

[14] O. Aourik, A. Chouaf, M. Othmani, Analysis of the resistance to crack propagation in SENT test specimens printed in ABS using parallel or crossed filaments between layers, Frattura ed Integrità Strutturale 17/63 (2022) 246-256. DOI: https://doi.org/10.3221/IGF-ESIS.63.19

[15] S.H. Ahn, M. Montero, D. Odell, S. Roundy, P.K. Wright, Anisotropic material properties of fused deposition modeling ABS, Rapid Prototyping Journal 8/4 (2002) 248-257. DOI: https://doi.org/10.1108/13552540210441166

[16] J.R. Rice, A path independent integral and the approximate analysis of strain concentration by notches and cracks, Journal of Applied Mechanics 35/2 (1968) 379-386. DOI: https://doi.org/10.1115/1.3601206

[17] ASTM D6068-96(2002)e1, Standard Test Method for Determining JR Curves of Plastic Materials, ASTM International, West Conshohocken, PA, 2010. DOI: https://doi.org/10.1520/D6068-96R02E01

[18] J.G. Merkle, H.T. Corten, A *J* integral analysis for the compact specimen considering axial force as well as bending effects, Journal of Pressure Vessel Technology 96/4 (1974) 286-292. DOI: https://doi.org/10.1115/1.3454183

[19] G. Clarke, J. Landes, Evaluation of the J Integral for the Compact Specimen, Journal of Testing and Evaluation 7/5 (1979) 1-6. DOI: https://doi.org/10.1520/JTE10222J

[20] ISO 13586:2018, Plastics. Determination of Fracture Toughness (GIC and KIC). Linear Elastic Fracture Mechanics (LEFM) Approach, International Organization for Standardization, Geneva, 2018.

[21] ASTM D5045-99, Standard Test Methods for Plane-Strain Fracture Toughness and Strain Energy Release Rate of Plastic Materials, ASTM International, West Conshohocken, PA, 1999. DOI: https://doi.org/10.1520/D5045-99

[22] ASTM E813-81, Standard Test Method for J_{IC}, a Measure of Fracture Toughness, Annual Book of ASTM Standards, Part 10, Philadelphia, PA, 1981, 810.

[23] O.O. Santana, C. Rodríguez, J. Belzunce, J. Gámez-Pérez, F. Carrasco, M.L. Maspoch, Fracture behaviour of de-aged poly (lactic acid) assessed by essential work of fracture and J-Integral methods, Polymer Testing 29/8 (2010). 984-990. DOI: https://doi.org/10.1016/j.polymertesting.2010.09.004

[24] M.R. Ayatollahi, A. Nabavi-Kivi, B. Bahrami, M.Y. Yahya, M.R. Khosravani, The influence of in-plane raster angle on tensile and fracture strengths of 3D-printed PLA specimens, Engineering Fracture Mechanics 237 (2020) 107225. DOI: https://doi.org/10.1016/j.engfracmech.2020.107225

[25] A. Andrzejewska, Ł. Pejkowski, T. Topoliński, Tensile and fatigue behavior of additive manufactured polylactide, 3D Printing and Additive Manufacturing 6/5 (2019) 272-280. DOI: https://doi.org/10.1089/3dp.2017.0154

[26] L. Gao, A.D. Drozdov, The Use of Various Measurement Methods for Estimating the Fracture Energy of PLA (Polylactic Acid), Materials 15/23 (2022) 8623. DOI: https://doi.org/10.3390/ma15238623